IEEE Access
Multidisciplinary ⋮ Rapid Review ⋮ Open Access Journal

Received 17 May 2024, accepted 29 May 2024, date of publication 6 June 2024, date of current version 14 June 2024.

Digital Object Identifier 10.1109/ACCESS.2024.3410547

TOPICAL REVIEW

Bioimpedance Sensing and Ablation Needles for Image-Guided Therapy

YIJIANG HU[1], CHAYABHAN LIMPABANDHU[1], TRISTAN BARRETT[2], AND ZION TSZ HO TSE[1]
[1]Centre for Bioengineering, School of Engineering and Materials Science, Queen Mary University of London, E1 4NS London, U.K.
[2]Department of Radiology, School of Clinical Medicine, University of Cambridge, CB2 0QQ Cambridge, U.K.

Corresponding author: Zion Tsz Ho Tse (z.tse@qmul.ac.uk)

This work was supported in part by the Academy of Medical Sciences Professorship under Grant APR6\1011, in part by the Royal Society Wolfson Fellowship under Grant RSWF\FT\191015, in part by Cancer Research U.K. under Grant EDDPMA-Nov21\100026, in part by the National Institutes of Health (NIH) Bench-to-Bedside Award, in part by the NIH Center for Interventional Oncology under Grant ZID BC011242 and Grant CL040015, and in part by the Intramural Research Program of NIH.

ABSTRACT Sensing and ablation needles and catheter instruments combined with multimodal imaging, navigation and AI-assisted diagnosis have been increasingly utilised by interventional radiologists for image-guided therapy, emerging as an innovative tool for both diagnosis and treatment. This paper reviews the significant advancements in the field over the past decade, focusing on the development and refinement of both bioimpedance sensing needles and thermal ablation needles. Bioimpedance sensing needles differentiate pathological tissues by measuring impedance variations in biological tissues, offering a less invasive diagnostic approach. Thermal ablation needles, on the other hand, employ Radio Frequency (RF) techniques or Electrolytic Ablation (EA) to effectively target and treat lesions. This review covers the evolution of these needles, including advancements in materials, novel sensor technologies, impedance analysis methods, ablation catheter powering techniques, and needle design. It also provides insights into the needle structure, fabrication methods, and testing outcomes of these advanced sensing and ablation needles. Additionally, the paper presents an analysis of bioimpedance data across various pathological tissues and discusses innovative impedance analysis methodologies. The review concludes by presenting the current challenges in the field and discussing directions for future research, thereby providing an overview of the state-of-the-art in electronic technology for medical diagnosis and treatment needles.

INDEX TERMS Bioimpedance sensing, radiofrequency ablation, bioimpedance cancer.

I. INTRODUCTION

According to Global Cancer Statistics 2023, roughly 19-20 million people are diagnosed with cancer yearly, and approximately 10 million die from cancer [1]. Novel cancer therapies have grown significantly in recent decades, and early cancer detection and therapy have improved cancer patient survival [2]. Thus, cancer therapy requires early cancer identification. Screening tests, cancer biomarkers, imaging, and biopsy are examples of early cancer detection methods [3], [4], [5], [6]. The biopsy procedure is one of the commonly used approaches to more definitely diagnose cancer, wherein a biopsy needle is inserted to take a small sample of body tissue. However, conventional biopsy procedures entail risks such as bleeding, infection, and damage to the organs. Moreover, the patients must wait a few days for the biopsy results. Therefore, developing a new biopsy cancer diagnosis system to overcome the previous limitations of conventional biopsy is of clear clinical benefit. In the past decades, researchers have demonstrated that cancerous tissues' electricity properties are different from normal tissue [7], and further research has been published utilising bioimpedance for clinical diagnosis [8], [9], [10], [11]. Based on these theories, several novel electronic biopsy needles were researched to detect pathological tissues in real-time by monitoring the impedance parameters [7], [12], [13], [14], [15]. Bioimpedance can be measured by electrode configuration on the electronic sensing needle [11] and using

The associate editor coordinating the review of this manuscript and approving it for publication was Paolo Crippa.

a fine needle as the detector can minimise damage to viscera and vascular tissues during the procedure.

Electrical Impedance Spectroscopy (EIS) is a crucial technique to characterise the bioimpedance of bio-tissues measured in different frequencies of AC-current [13], [14], [16], [17], [18], [19], leading to improved tissue detection accuracy [15], [16], [17], [20]. Moreover, EIS can provide massive impedance data from bio-tissues, allowing advanced algorithms and data analysers to better classify different bio-tissues. Furthermore, EIS also provides the potential for Machine Learning models to diagnose cancer in the future [21].

Tumour ablation is another efficient oncological treatment method. Needle-based ablation devices offer a minimally invasive approach, with thermal and non-thermal ablation improving over the past decade. Thermal ablation is a minimally invasive medical procedure that uses a radiofrequency (RF) catheter to heat the lesional tissue to a cytotoxic temperature. Conversely, non-thermal ablation uses other methods of promoting cell structure destruction, such as lowering the pH of cancer cells using electrolytic ablation [22].

This review article focuses on bioimpedance sensing needles and ablation needles for cancer diagnosis and treatment. Further potential clinical usage of biopsy electronic needles will also be introduced.

II. METHODOLOGY

The keywords "Impedance sensing RF needle", "Radiofrequency ablation", and "Bioimpedance cancer diagnosis" were used in the specific search engine Google Scholar for articles published between March 2013 and March 2023. In total, 118 initial papers were generated for reviewed, of which 57 were related to clinical radiofrequency technologies. Subsequently, papers discussing the novel bioimpedance sensing approaches for cancer detection and RF ablation were selected, leaving 29 papers for the purposes of our review (Figure 1).

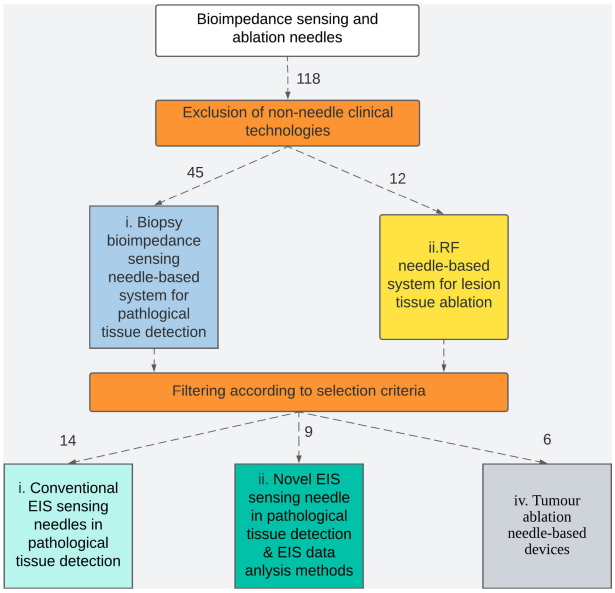

FIGURE 1. Process of selecting papers in this article.

III. MATH NEEDLE-BASED DEVICES IN PATHOLOGICAL TISSUE DETECTION

According to a previous work [8], changes in cell structure, fluid state, and electrical current can impact tissue conductivity and impedance. Therefore, bio-impedance analysis can be a potential method to characterise bio-tissue properties. Impedance is the opposition of current flow, which includes resistance and reactance, usually represented by Z. Resistance of a linear resistor where resistivity is constant does not change with AC frequency, but resistance which is a real impedance component does. Reactance can be classified as capacitive reactance (X_C) or inductive reactance (X_L). Table 1 shows the relationship between the reactance, frequency (f), capacitance (C) and inductance (L) and the explanations of all parameters used in this paper.

The inductive reactance can also be calculated as impedance and represented as a complex number with the same unit as resistance (ohm). Different from resistance, reactance is the imaginary part of the impedance. The real part and imaginary part of the impedance are usually represented as $\boldsymbol{Re}[\boldsymbol{Z}]$ an $\boldsymbol{Im}[\boldsymbol{Z}]$, respectively. These variables are significant for characterising the electrical properties of bio-tissues. The measurement of impedance is obtained by applying electrical potential waves (E) to the electrodes and recording the resulting current waves (i) and calculate with the formula in table 1. Electrochemical Impedance Spectroscopy (EIS) is a crucial technique to characterise impedance variation of bio-tissues, which can be used to analyse interfacial properties related to bio-recognition events occurring at the electrode surface and characterise the electrical property of biological objects by generating the spectrums of impedance variables at different frequency ranges [25].

A. APPLICATIONS OF CONVENTIONAL SENSING NEEDLES AND BIOIMPEDANCE ANALYSIS METHODS

Conventional sensing needles are currently deployed in the commercial sector. Their structure usually consists of an inner element (a metal wire or an inner needle) and an outer element (the needle cannula), and they are electrically insulated as a pair of bipolar electrodes. In clinical practice, the bioimpedance measurement methods consist of monopolar and bipolar setups. Sharp et al. conducted a comparative study to evaluate these two different setups in the biopsy procedure [22]. An in-vivo experiment on pork was conducted to test monopolar and bipolar needles. Unlike the bipolar setup, the sensing needle in the monopolar setup only contains one electrode on the needle tip, and another reference electrode was placed on the pork's skin. The impedance of nerve tissue and cerebrospinal fluid from a piece of pork was measured by monopolar and bipolar

TABLE 1. Explanations and formulas of technical parameters.

Symbol	Definition	Formula	Unit
j	Imaginary unit	$j=\sqrt{-1}$	N/A
q	Electrical charge	N/A	Columb
E	Electrical potential waves	N/A	V
i	Electrical current	N/A	A
f	Frequency	N/A	Hz
C	Capacitance	$C=\frac{q}{V}$	F
L	Inductance	$L=\frac{Z}{jw}$	H
R	Resistance	$R=\frac{V}{i}$	Ω
$\boldsymbol{j}$	Imaginary unit	$\boldsymbol{j}=\sqrt{-1}$	N/A
Z	Impedance	$Z=R+j(X_L-X_L)=\frac{E}{i}$	Ω
X_C	Capacitive reactance	$\frac{1}{2\pi fC}$	Ω
X_L	Inductive reactance	$2\pi fL$	Ω
θ	Impedance phase angle	$\theta=\tan^{-1}\frac{(X_L-X_C)}{R}$	°
M	Impedance magnitude	$M=\lvert Z\rvert=\sqrt{R^2+(X_L-X_C)^2}$	Ω
$\boldsymbol{Re[Z]}$	Impedance magnitude	$\boldsymbol{Re[Z]}=R$	Ω
$\boldsymbol{Im[Z]}$	Impedance imaginary part	$\boldsymbol{Im[Z]}=j(X_L-X_L)$	Ω
$\boldsymbol{l}$	Range of sensing area	**N/A**	m
$\boldsymbol{\rho_R}$	Resistive bioimpedance parameter	$\boldsymbol{\rho_R}=\frac{X_C}{\boldsymbol{l}}$	Ω-m
$\boldsymbol{\rho_X}$	Reactive bioimpedance parameter	$\boldsymbol{\rho_R}=\frac{X_L}{\boldsymbol{l}}$	Ω-m
$\boldsymbol{Y'}$	Real part of admittance	$\boldsymbol{Y'}=\frac{\mathbf{1}}{\boldsymbol{Re[Z]}}$	S
$\boldsymbol{Y''}$	Imaginary part of admittance	$\boldsymbol{Y''}=\frac{\mathbf{1}}{\boldsymbol{Im[Z]}}$	S

setups. According to the experimental results, both setups work similarly in inhomogeneous volumes such as biological tissue. However, the current path in the bipolar setup is localised to the smaller tissue volume between two electrodes compared to the monopolar setup. Due to this, the bipolar setup is unaffected by other metal implants in the patient's body. Therefore, a bipolar setup is slightly better than a monopolar setup.

Halonen et al. conducted a human in vivo liver tumour bioimpedance measurement experiment [23]. They sent 1ms (millisecond) long pulse voltage excitation signals from 7Hz to 349kHz by a bioimpedance biopsy needle (IQ-Biopsy, Injeq Oy, Tampere Finland) to measure the impedance spectra of the in-vivo normal liver tissue and tumour tissue from patients, and 50% trimmed mean values of magnitude and phase angle were collected as the tissue distinction reference. The experimental results indicated that the trimmed mean values of the phase angle of tumour tissue (approximate from $-59.8° \pm 0.1°$ to $-24° \pm 0.5°$) were lower than that of normal liver tissue (approximate from $-55° \pm 0.5°$ to $-25° \pm 0.5°$) at a frequency range of 10 kHz to 17kHz, and less negative (approximate from $-23° \pm 0.5°$ to $-15° \pm 0.5°$) than that of normal liver tissue (approximate $-25°$ to $-13°$) at higher frequency range of 17kHz to 349kHz. Moreover, the magnitude of liver tissues (14kΩ to 2.5kΩ) was generally higher than that of liver tumours (12.5kΩ to 2.4kΩ) in the impedance spectrum, with the phase angle providing higher differentiation than magnitude at a frequency >30kHz (p-value<0.05). Within a frequency of 7Hz-23kHz, the impedance magnitude provided higher differentiation than the phase angle (p-value<0.05). The authors acknowledge that the main limitation was that they could not directly compare to the data obtained by another device due to the difference in configuration of the measuring electrodes/devices affecting the measurement of impedance.

Maglioli et al. detected the bioimpedance of six different animal organ tissue samples and six different tissue parts from an ex-vivo porcine larynx body using a new small size needle-based bioimpedance sensing system [12]. The system consisted of an impedance converter based on chip AD5933, a commercial single-use sterile concentric electrode needle, and an Arduino DUE. Impedance of tissue samples was measured by excitation frequencies ranging from 10kHz to 100kHz, at 200Hz increments. The sum of Squared Differences (SSD) of an average value of impedance magnitude and phase angle at each increment was collected, and a bioimpedance magnitude-phase graph at the frequency of 100kHz was made for tissue distinction. The experimental results showed that SSD of magnitude and phase angle were increased and reached the maximum value with frequencies > 70kHz, indicating this threshold could potentially provide good tissue distinction. Furthermore, the Bioimpedance Magnitude-Phase graphs demonstrated different tissue samples well, with the data sets not overlapping. These results suggest that healthy laryngeal tissue presents characteristic bioimpedance values which allow discrimination through a combined analysis of magnitude and phase angle. One significant feature of this system is that most of its hardware was created by commercialised components, making it more possible to apply the system in industry, however, the system still requires evaluation for accuracy and safety by further experiments related to human body tissue.

Cheng et al. also created a small needle-based bioimpedance sensing system called SmartProbe to study the bioimpedance characteristics of pathologic and healthy tissues from the head and neck region [24]. The core components of SmartProbe consist of a commercialised EMG

needle, an impedance converter based on chip AD5933, and an Arduino DUE. The impedance of four types of human ex-vivo cancerous tissue and normal tissue from the head and neck (muscle, mucosa, cartilage, and salivary gland) were evaluated by an excitation signal in the frequency range of 10kHz to 100kHz, at 10kHz increments. They analysed the values of conductivity and phase angle. According to the principal component analysis (PAC) based on the impedance spectrums, healthy neck tissues generally have a higher conductivity than cancerous tissue, and the phase angle may not contribute significantly to tissue classification because the values of phase angle of both tissue sets overlapped in the impedance spectrum. Results from T-test indicated that cartilage (p-value $= 0.0178$), muscle (p-value $= 1.589 \times 10^{-12}$), and mucosa (p-value $= 2.514 \times 10^{-5}$) can be successfully classified by conductivity change, but the device still faced challenges to classify salivary gland tissues (p-value $= 0.4701$).

Kwon et al. developed a new tetrapolar sensing needle that applied electrical impedance myography (EIM) to detect lesion muscle in neuromuscular disease [27]. The new needle contained two current and two voltage ring shape electrodes to measure the apparent impedance per unit length (apparent impedivity). In-vivo experiments used five healthy mice (DBA/2-congenic dmd-mdx mice) compared to five mice with muscular dystrophy (wild-type control DBA/2J mice) to test the muscle sensing capability of the EIM needle. The apparent impedivity of the two groups was measured by the needle with an excitation signal in a frequency range of 10kHz to 1MHz. Comparison of experimental results between two groups of mice indicated that the optimal discrimination frequency of the needle was 10kHz when the apparent resistivity and apparent reactivity values of the dystrophic mice group and healthy mice group demonstrated significant differences ($p<0.05$, and $p<0.005$, respectively).

Kalvøy and Sauter researched an approach for discriminating nerve tissue from other tissue types based on multiple frequency impedance measurements [28]. They created a novel algorithm based on principal component analysis (PCA) to analyse parameters impedance modulus and phase angles. Moreover, two new variables, Delta phase angle and Compound variable C derived from the PCA plot were used as tissue discrimination parameters. Where the Compound variable C is a variable that distinguishes different nerves, combining the impedance modulus and phase values within a particular formula. A 3-electrode needle-based setup was used to measure the bioimpedance of sciatic nerve tissue of eight 3-month-old pigs by sending sine wave excitation signals in a frequency range of 1.26 to 398kHz. The result showed that the sensitivity rates for four parameters were modulus (78%), Phase angle (86%), Delta (94%), and C (97%). Therefore, PCA and new Compound variable C can improve the sensitivity of nerve tissue discrimination.

The earliest report about the application of an EIS sensing needle is from Mishra et al., who created an EIS sensing biopsy (EIS-Bx) needle-based device aimed to provide additional information from tissues by monitoring the impedance spectra [20]. The sensing needle was reconstructed based on a commercial biopsy instrument (BARD Maxcore Disposable Biopsy Instrument) and comprised bipolar electrode configuration. An ex-vivo experiment tested the validation of its clinical use. They used the EIS-Bx device to record the bioimpedance spectrum from 432 cancerous prostate tissue cores from 36 men (12 cores per person), using a broader frequency range of 100 Hz to 1 MHz than previous experiments [15]. Impedance spectrum of tissues analysis by restive and reactive components, where the resistive component describes how easily current passes the tissue, and the reactive component presents the bio-tissue charge storage capability. The results indicated that the mean value of a resistive component of cancer tissue decreased from 67.8Ω-m (100Hz) to 4.52Ω-m (1MHz), and that of normal tissue decreased from 42.8 Ω-m (100Hz) to 2.48 Ω-m (1MHz). Meanwhile, the mean value of the reactive component in the miniguide form of cancer tissue decreased from −92.9 Ω-m (100Hz) to −4.48 Ω-m (1MHz), and that of normal tissue decreased from −49.68 Ω-m (100Hz) to −1.11 Ω-m (1MHz). The result illustrated that prostate cancer tissue presented less conductivity and higher charge storage capability than normal tissue. The optimal frequency to identify cancer tissue was 63.09kHz for the resistive component and 251.1kHz for the reactive component. At these optimal frequencies, the resistive component provided a specificity of 75.4%, and the reactive component provided a sensitivity of 71.4%. Furthermore, the EIS-Bx needle has radial and axial sensitivities of around 4 and 3mm. However, the experiment only analysed the impedance spectrum based on histopathological assessment of the tissue core extracted. While in practice, the EIS-Bx device was found it challenging to identify tissue surrounding the needle tip. Hence, further improvement of its accuracy is required for clinical use.

A novel approach that combined EIS for needle guidance in intra-articular injection therapy is presented by Abbasi et al. [29]. A discrete Fourier Transform (DFT) impedance analysis system based on a monopolar needle and an AD5933 impedance converter was set up to record the EIS of intra-articular space tissues of the elbow joint and the knee joint from a 7-month-old female pig. An excitation signal from 10Hz to 100kHz was applied in an in-vivo measurement. A novel algorithm that used a digital low-pass filter in EIS analysis was developed for tissue discrimination. The algorithm was designed to monitor the impedance changes during the needle insertion by calculating the sampled data from the impedance spectrum with a 30 ms interval. Experimental results showed that during the knee joint injection at frequency 100kHz, the subcutaneous tissue presented a higher impedance magnitude (5100Ω to 5250Ω) than intra-articular space (around 1700Ω). In the elbow joint of the pig, the difference in impedance magnitude of subcutaneous fat and intra-articular space was minimal

(Standard Deviation less than 8Ω) compared to the knee joint. They compared this novel method with ultrasonography and conventional anatomical guidance and indicated that real-time impedance monitoring in intra-articular space detection provided higher accuracy (99%) than the other two conventional methods (90% and 40%, respectively). Furthermore, the price of EIS detection is much lower (USD 10) than ultrasonography guidance (USD 8,340). As a result, a monopolar injection needle with EIS can potentially be a low-cost, highly accurate and real-time monitoring medical instrument for curing intra-articular space disease.

Mahdavi et al. created a system named Electrical Lymph Scoring (ELS) with EIS for Intraoperative pathologically calibrated diagnosis of breast cancer by analysing the electrical properties of lymph nodes (LNs) [17]. The ELS system consists of a needle-shaped 2-electrodes probe and an impedance analyser, and it works in two modes of non-neoadjuvant and neoadjuvant chemotherapy. The Z_{1kHz} (Impedance magnitude at 1kHz), and IPS (impedance phase slope in the frequency ranges of 100kHz-500kHz) are the classification parameters for non-neoadjuvant mode, and Y'_n (normalised real part admittance of the extremum point in Nyquist diagram) is the classification parameter for neoadjuvant mode. Impedance spectrum of 282 dissected LNs from 77 patients was measured and analysed by ELS system in corresponding modes, of whom 55 were under non-neoadjuvant treatment and 22 were under neoadjuvant treatment. The experimental results showed that Z_{1kHz} of most cancer-involved LNs from non-neoadjuvant patients were below 2.3kΩ with IPS between −10 and 0 or below 2.3 Ω with IPS between −12 and −10, where most normal LNs from patients presented larger with an IPS between −20 to −5. The of the classification parameters from LNs involved and not involved cancer was strongly significant (p-value = 7.2E-25). The LNs from neoadjuvant classified by Y'_n, where the extremum point was mainly above 0.85 in normal LNs and less than 0.85 in neoadjuvant LNs involved by cancerous cells according to the test result from Y'_n. As a result, the novel ELS system was evaluated to have a detection sensitivity of 95% (p<0.001) and 91% (p<0.001) of non-neoadjuvant and neoadjuvant breast cancer cases, respectively.

B. APPLICATIONS OF THE NOVEL SENSING NEEDLE IN PATHOLOGICAL TISSUE DETECTION

Improvement of the bipolar electrodes was presented by Yun et al., who created a novel needle named EIS on a needle (EoN) by fabricating the bipolar interdigitated electrode (IDE) on the end of a curved surface of a hypodermic needle (Figure 2a) [30]. IDE is fabricated by wet etching the Cr/Au film on the surface of the hypodermic needle, which makes the electrodes have a minimal size (maximum width of 400μm) on the needle surface and a film photomask coated on the needle's surface to avoid peeling off the electrodes when bio-tissues are penetrated. The EoN contained a detection part (needle tip embedded IDE), a connection part (straight electrodes), and a needle hub (a Printed Circuit Board contains multiple output ports). A classification parameter named discrimination index (DI) was calculated based on the standard deviation values of

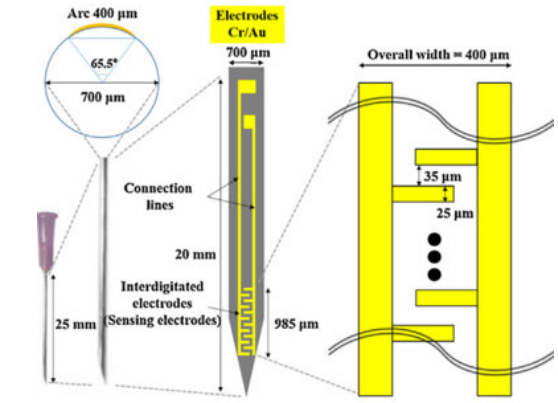

(a) Structural details of the EoN with IDEs at the end of a 22-gauge hypodermic needle [28].

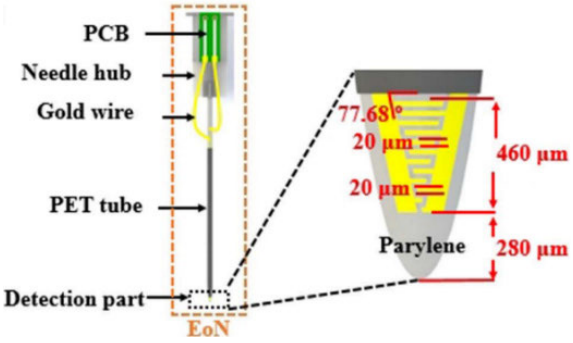

(c) schematic design of EoN, comprising of a detection part [29]

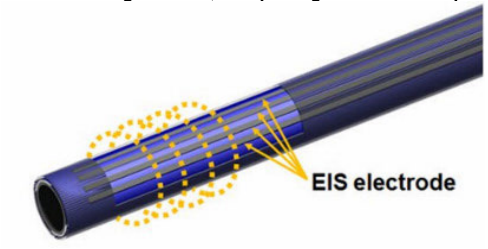

(d) Overall structure of biopsy needle [25]

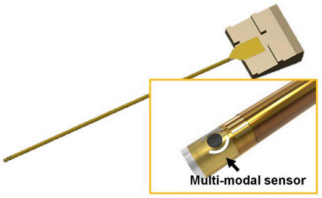

Multi-modal sensor integrated biopsy needle

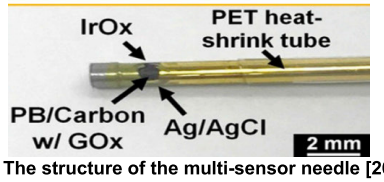

(d) The structure of the multi-sensor needle [26].

FIGURE 2. Novel impedance sensing needles.

magnitude and phase angle. The higher the value of DI, the more significant the differences in the electrical properties of tested tissues. A three-layers (fat, muscle, and fat) porcine tissue sample was utilised for the experiments. The results of measurement showed that the needle performed the highest DIs to distinguish first-layer tissue and second-layer tissue at 627Hz (15.772), 111Hz (6.978), 627Hz (15.686), and 100Hz (5.235) in the order of real part and imaginary part of impedance, magnitude, and phase. The highest DIs to distinguish the second layer and third-layer tissue were observed at 111Hz (1.097,1.648, and 1.284) and 177Hz (0.368) in the same order. However, a limitation of the EoN is that its connection part can be affected by the passed bio-tissues during puncturing, causing a considerable distortion in the sensor output and decreasing the accuracy of measurement. To overcome this limitation, they created a method named as incremental compensation method (ICM) [29], the mechanism of ICM is that in the process of EoN puncturing into bio-tissue, the impedance values extracted on the detection part and connection part (immersion depth 3.42mm) will be recorded as the key result. The critical result will replace the later impedance values extracted from EoN in deeper insertion (bio-tissue wholly immersed in the connection part). To evaluate the accuracy enhancement of ICM, they tested two sets of EoN (one applied ICM) by measuring the conductivity of phosphate buffer of phosphate buffer saline (PBS) solution with six different concentrations. The experimental results indicated that the detection accuracies for the conductivity and relative permittivity of the PBS were enhanced by 5.59 times and 2.18 times, respectively when EoN used ICM. However, ICM limits the maximum insertion depth of the needle to 12.42 mm, and its enhancement is only evaluated by EoN with PBS solution instead of a bio-tissue sample. Therefore, using insulating materials on the connection part is a consideration in order to avoid the output error caused by the connection partly immersed with tissues, and it is easier to apply in different types of sensing needles.

Yun et al. conducted an ex-vivo experiment to identify thyroid cancer tissue by using EoN [13]. 13 papillary thyroid carcinoma (PTC) tumour and normal thyroid tissue specimens taken from 13 patients, were used in experiment. A 1Hz to 1MHz impedance sweeping for the specimens was accomplished specimens by an impedance analyser connected to the EoN via a PCB needle hub. From the results, largest DI of impedance were observed to be 1.02 at 631kHz for magnitude, 0.88 at 15.9kHz for phase, 1.03 at 251kHz for *Re[Z]* and 0.71 at 1MHz for *Im[Z]*, respectively. To distinguish cancer tissue and normal tissue, a threshold value was obtained by measuring the impedance of normal tissue at optimal distinguishing frequency, then compare the impedance values from deeper penetration with the threshold value. The maximum sensitivity and specificity were found to be 78.2% and 85.3% of EoN in this experiment. The challenge of this method is taking a correct threshold value at the beginning of biopsy procedure. In practice, it is difficult for doctors to identify if the needle tip is punctured into normal or pathological tissue via ultrasound guideline.

Kang et al. further improved the IDE by applying a newly developed flexible photomask: Parylene-C film, in the fabrication process (figure 2b) [16]. Two types of EoN were designed and fabricated for the comparison experiments, and they were classified into open type (electrodes of open type are exposed to the air) and passivation type (Parylene-C passivates electrodes of passivation type). Furthermore, ex-vivo experiments used PBS solution to test the capabilities of detecting the electrical properties of new needles. Skin, fat, and muscle of pork, human healthy tissue and three cancer grades (grade I, II, II) of cancerous breast tissues from females were used to test the tissue discrimination capability of the new needles. Constant excitation voltage was applied to characterise the electrical properties of the bio-tissues in the frequency range from 1kHz to 1MHz. The results from the porcine tissues experiment indicated that both needles could clearly distinguish skin, muscle, and fat tissues within the p-value of less than 0.001. Moreover, the open type showed higher performance in accuracy, and the passivation type showed higher precision during the measurement of the conductivity of porcine tissues. In breast cancer discrimination, the resistance performed better differentiation in discriminating all types of breast cancer than reactance. DIs obtained by resistance value from both types were 4.11 (4.71), 6.84 (5.13), and 7.01 (5.86), corresponding to cancer grade I, II, and III of passivation type and open type, respectively. DIs from the passivation type were generally more extensive than the open type, making it superior to the open type in cancer tissue discrimination.

Yun et al. researched EIS data from renal tissues obtained from each of 10 Renal Cell Carcinoma patient by using EoN [14]. They measured the impedance values of ex-vivo specimens of normal and cancerous renal cells over the frequency ranges from 100Hz to 1MHz. The experimental results showed the mean values of impedance magnitude and phase angle of normal tissue were $5013 \pm 94.39\ \Omega$ and $68.54 \pm 0.72°$, and those of cancer tissues were $4165.19 \pm 70.32\ \Omega$ and $64.10 \pm 0.52°$, respectively. Generally, the magnitude of cancer tissue was lower than that of normal tissue, and the phase angle of both cancer and normal tissue overlapped on the impedance spectra. They obtained the optimal frequency of cancer discrimination by using a magnitude of 1MHz, which provided the highest DI (5.15 at 1MHz), with an optimal frequency for phase angle of 1kHz providing the best DI (3.57 at 1kHz). The results highlighted the potential of EoN in clinical use for renal cancer diagnosis. Further validation of its safety and sensitivity requires further in vivo human trials.

Kim et al. researched the utilisation of an improved EoN in EIS analysis of hepatocellular carcinomas (HCC), cirrhotic liver parenchyma (CLP), normal liver parenchyma (NLP), and metastatic tumour normal liver (MLT) in human ex-vivo normal liver and in human ex-vivo cirrhotic liver [31]. The new EoN was comprised of IDE and straight electrodes

(SEs). Comparing the previous model of EoN in [30], they replaced the IDE's rectangular shape with a triangular shape, significantly reducing the distance between the detection electrode and sharp tip to 280μm, which further minimised the intrahepatic visceral or vascular damage (Figure 2c). The impedance parameters of HCC, CLP, NLP, and MLT bio-tissue samples were measured by excitation signal in a frequency from 100Hz to 1 MHz. The optimal frequency range for tissue discrimination was 0.46 MHz to 1MHz (p-value <0.05) observed from the experimental results. The largest DIs were obtained at 1MHz, 2.71 and 0.96 in the real and imaginary parts of impedance between CLP and HCC, respectively (p-value <0.01). And the highest DIs of real and imaginary parts for NLP and MTN were 3.62 and 2.54, respectively (p-value <0.01). These results imply the potential of EoN as a tool to locate a malignant tumour in the liver and apply it in Percutaneous Ethanol Injection (PEI) or Fine Needle Aspiration Biopsy (FNA) procedures.

However, the measuring accuracy of 2-electrode sensing needles is likely to be affected by the electrode polarisation (EP) with AC frequency less than 100kHz, where the EP caused by the attracted ions in bio-tissue near the electrodes and generates an electrical double layer. To overcome this limitation, Park et al. created a new biopsy needle integrated with a novel EIS microelectrode array on the needle's surface to decrease the EP effect during measurement (Figure 2d) [25]. The microelectrode array consisted of a 4-electrode configuration, and the whole sensing needle consisted of a stainless-steel needle with a diameter of 1.2mm (gauge 18) and a length of 15cm. Saline solutions with different concentrations and the fatty and normal mice livers were used to mimic alcoholic fatty liver disease to test the new needle's accuracy and tissue distinction capability. The results of solution tests showed that the 4-electrode showed less relative error than the 2-electrode during the measurement, while the results of the murine experiments showed that the conductivity of the standard mouse liver increased from 0.1095 S/m (1kHz) to 0.4177 S/m (1MHz), and that of the fatty mouse liver increased from 0.0864 S/m (1kHz) to 0.1842 S/m (1MHz). In general, the fatty mouse liver has less conductivity. From the impedance spectrum, the differences between two types of liver tissues can be observed with significance, showing promise for the new needle to distinguish different types of tissues. One limitation of the new needle is that parasitic impedance can be generated in the microelectrode patterning process. Therefore, further research on proper fabrication is required.

To utilise the biochemical differentiation between cancerous and healthy tissue as mentioned by previous reports [32], [33], [34], [35], Park et al. created a novel biopsy needle integrated with multi-model sensors (Iridium oxide-based pH sensor, enzymatic glucose sensor, and Au electrode) which focuses on detecting pH changes, electrical conductivity, and glucose concentration of bio-tissues (Figure 2e) [26]. The needle was tested using PBS solutions, and glucose solutions with different glucose concentrations and pH values. The results of solution tests indicated that the Au electrode performed a relative error of less than 15%, the IrOx-based pH sensor presented a sensitivity of 69.3mV/pH and the enzymatic glucose sensor presented an average sensitivity of -4.47nA/mM. In the tissue classification experiment, an ex-vivo porcine liver with exchanged internal parameters (pH, glucose concentration) was used to mimic the cancerous tissues.

Meanwhile, multiple solutions with the same parameter value as porcine liver were prepared for the comparison test. The porcine liver experiment evaluated that the detection accuracy of a needle was almost the same as the detection accuracy from the comparison tests. Based on the results, the novel needle has massive potential in cancerous tissue detection based on more classification parameters.

Lin et al. created a needle-integrated ultrathin bioimpedance microsensor array to detect early extravasation during intravenous therapy [36]. The biopsy needle with a 50 μm 8-electrodes sensor arrays fabricated by using photolithography to pattern Au electrodes on a flexible polyimide substrate and electrochemical deposition to coat them with a porous PEDOT-MWCNT layer and integrate them on an 18-gauge medical-approved needle by using the epoxy adhesives (Figure 3a. Left). In-vivo, animal experiments evaluated the needle with an 8–12 week male wild-type mice. The result showed the most significant impedance variation caused by extravasation was detected when injected 100 μL 0.9% NaCl solution, the tissue impedance magnitude reduced from 36.1kΩ to 17.3 kΩ, but that of blood vessel remained at 50kΩ. Furthermore, the sensing needle was able to detect local impedance change with injecting as low as 20 μL. Therefore, impedance variation during intravenous therapy can be detect by the micro-electrode array subcutaneous solutions before visual assessment of skin swelling in a mouse model was possible and sensitively differentiated extravasation from conventional injections in a pig model. However, further clinical validation of the accuracy and safety of these microsensors is required for clinical use.

Another similar functioning needle device was created by Cheng et al. [37]. This device was designed to help in the peripheral intravenous catheterisation (PIVC) procedure by detecting bio-impedance differences in the skin, vein wall, and blood to identify the needle's entry into the patient's body. The device was developed based on a concentric electrode needle (CEN) (Figure 3a. Right) and an intelligent venous entry indicator (SVEI). The impedance of lateral veins from 15 rats was used in an in-vivo trial to evaluate the sensitivity of this device with an excitation frequency from 10 to 100kHz. The results indicated that the best blood identification excitation frequency was 100kHz based on the rat trial, where the impedance values of blood identification were real part less than 1.507kΩ and imaginary part larger than -1.497kΩ. A limitation of this study is that the optimal

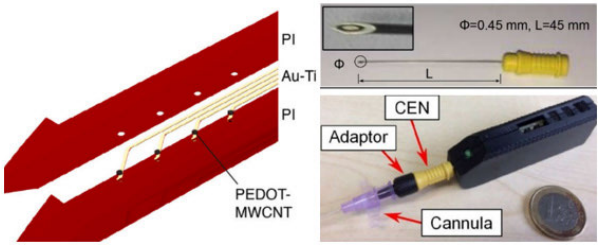

(a) Magnification of the commercial concentric type needle probe(Left) [36]. The needle structure and SEVI prototype (Right) [37].

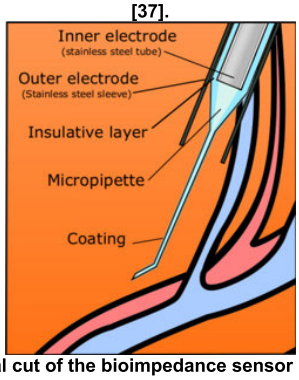

(b) Transversal cut of the bioimpedance sensor prototype [38].

FIGURE 3. Needles with bioimpedance sensors in medical trials.

excitation for blood detection frequency was observed at 100kHz, where the frequency is the maximum frequency provided by the impedance converter. Therefore, further trials at higher excitation frequency are required.

Schoevaerdts et al. created a needle device that applied a new impedance sensor to identify punctures of retinal vessels by detecting the impedance of blood [38]. The new sensor had inner and outer electrodes that were electrically insulated (Figure 3b). The principle of its impedance measurement is by injecting the conductive thrombolytic agent through the needle lumen in the eye and observing the impedance variation when the electrode touches the vessel wall. The impedance values of a pig eyeball were measured at 6kHz as an ex-vivo experiment. In total, the experiment executed 12 punctures, including five double punctures. The experimental results showed the impedance magnitude with a standard deviation of $\pm$ 0.660 kΩ, and the electrical sensitivity was tuned to optimise the impedance, both punctures and double punctures were recognised in 80% of the cases. A limitation of this study is all the values from eyeball vessel were measured at 6kHz, and developing an impedance analysis algorithm may help to increase the accuracy of detection.

C. COMBINATION OF MACHINE LEARNING IN TISSUE DISCRIMINATION WITH EIS

Jeong et al. proposed a novel method for discriminating between normal and cancerous tissue by combining EIS and Machine Learning (ML) techniques [21]. 6 ML models: Logistic Regression (LR), K-Nearest Neighbors (KNN), Decision Trees (DT), Random Forest (RF), Support Vector Machine (SVM), and Back-propagation Neural Networks (BPNN) were selected to distinguish the Normal (SV-HUC-1) and cancerous (TCCSUP) urothelial cell through EIS. They created a micro-dimensional-EIS device equipped with a pneumatic valve for flow cytometry and a pair of electrodes to measure the impedance of the cell lines. The standard (SV-HUC-1) and cancerous (TCCSUP) urothelial cell lines were separated into five samples and measured at five different frequencies (10, 50, 100, 500kHz, and 1MHz). In total,135 impedance datasets of TCCSUP and 101 impedance datasets of SV-HUC-1 cell lines were collected to feed the machine learning models as the feature vectors. The experimental results indicated that the RF performed the best on three of the five performance parameters, and it classified normal and cancerous cells with an accuracy of 91.7%, a precision of 92.9%, a specificity of 90.0%, and an F1-score of 93.8%.

IV. TUMOUR ABLATION NEEDLE-BASED DEVICES

RF ablation is a minimally invasive medical method to remove lesion tissue, and it has the advantages of low costs and less tissue damage; novel approaches to needle-based RF ablation systems are introduced in the following section.

Moore et al. studied the application of Magnetic Resonant in a wirelessly powered ablation device to achieve Liver radiofrequency ablation (RFA) [39]. The power is transmitted through a transmitting coil (12cm diameter and 3 turns) and a receiving coil (6cm diameter and 3 turns) by applying 180 Vpp sine wave voltage, with an ablation catheter connected to receiving coil (Figure 4a). During the ablation, the alternate current will be sent between the inside stylet component and external sheath component of the catheter and direct the targeted tumour to generate ablation heat. An evaluation experiment based on porcine liver was conducted, showing the maximum voltage and maximum power that can be received in receiving coil were 92Vpp and 60W (Two coils are parallel), respectively. The temperature of catheter can rise 64 to 102 degrees Celsius in 60 seconds, and the maximum power transfer efficiency was recorded as 49% during the animal ablation test. Moreover, the maximum ablation zone of this prototype was 20 mm sphere around the needle tip.

To study wireless RF ablation using fewer wires, Moore et al. decreased the diameter of transmitting coil and receiving coil [40]. The diameter of the transmitting coil and receiving coil was decreased from 12 cm to 10 cm and from 6cm to 5 cm, respectively. Meanwhile, the coil turns of the transmitting coil and receiving coil was increased from 3 turns to 12 turns and from 3 turns to 14 turns, respectively. Ex-vivo experiments based on bovine tissue were conducted to test the power-transferring capability of the new prototype. The experimental results indicated that the average maximum received power was 15W, the maximum ablation temperature was around 65 degrees, and the average maximum power transmission efficiency can be increased to 63.27%. The

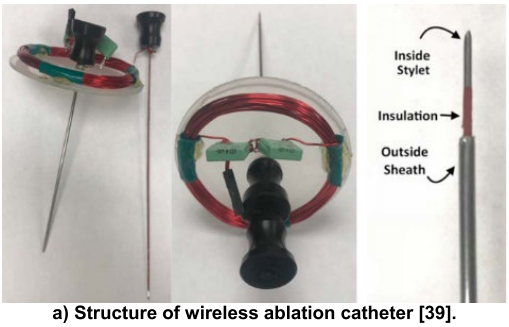

a) Structure of wireless ablation catheter [39].

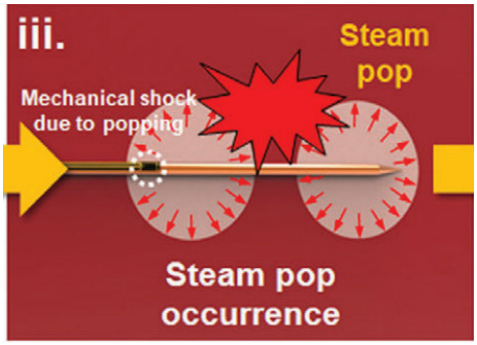

b) The Process of generating a steam pop during thermal ablating[43].

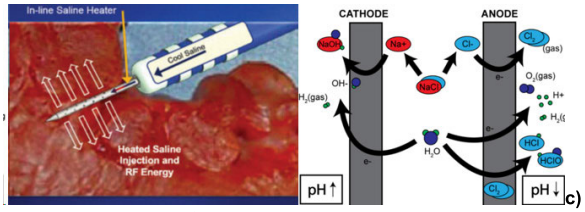

c) SERF ablation process.

FIGURE 4. Novel ablation catheters.

maximum ablation zone of this catheter was a cylinder with diameter of 12mm, height of 21mm. As the results showed, increasing coil turns can increase the power transmission efficiency, even though the diameter of both coils was smaller than that of the previous prototype.

Moris et al. researched a novel RF fine needle aspiration (EUS) catheter and endoscopic ultrasound in pancreatic cysts treatment [41]. A prototype of an RF EUS catheter was built by a 22-gauge monopolar needle with a tip electrode connected to a standard electrosurgical unit. The RF EUS ablation needle can provide a threshold of at least 60 °C and a safe cyst margin below 97 °C during the ablation tests in pancreatic cyst models. These results showed the potential of a commercialised EUS needle in RF ablation, implying that a low-cost, convenient, and simple RF ablation system could be applied for clinical use.

Another study into thermal ablation was presented by Dickow et al., who researched the two-dimensional intracardiac echocardiographic (2D-ICE) to guide and validate Saline-enhanced RF (SERF) needle ablation in real-time [42]. The SERF catheter had four distal-tip electrodes, and the stainless-steel ablation needle was fitted to the distal catheter (Figure 4c. Left). Compared to conventional RF ablation, SERF ablation can create larger ablation zones but more often transmural; creating controllable transmural lesions is essential, and real time monitoring by 2D-ICE is a way to achieve this aim using a 2D-ICE system constructed by a 64-element 5-10MHz catheter. An in vivo experiment using 11 mongrel dogs was conducted. The experimental results showed that the sensitivity, specificity, positive predictive value, and negative predictive value of transmural lesion were 70%, 47%, 74%, and 59% when using 2D-ICE, implying its suitability for SERF ablation. However, some cases of 2D-ICE imaging stack into the right ventricle were not achieved due to operator errors. Those errors limited the correlation between acute tissues and tissue lesions characteristics. Moreover, the test results were based on canine cardiac anatomy, and may not directly translate to human cardiac anatomy.

Many reports note that an unintended audible explosion, called ‘‘steam pop’’, may occur inside tissue during an RFA procedure. This phenomenon can induce various thermal and mechanical effects on neighbouring tissue [44], [45], [46]. Therefore, Park et al. created a sensor-integrated RFA needle (sRFA) (figure 4b) and aimed to predict the occurrence of steam pops [43]. A flexible sensor based on a polymeric platform with pressure and temperature sensing capabilities was integrated into the surface of the RFA needle. The sRFA needle comprised an internal tube and a thermocouple to maintain the temperature as low as possible (figure 4c). The steam pop detection test utilised a porcine liver and indicated that the sRFA needle could provide insight into the environmental changes during RFA. However, the needle was still unable to give a reliable prediction of the occurrence of a steam pop.

Another method to avoid ‘‘steam pops’’ is non-thermal ablation. Therefore, Kim et al. created an ultrasonically powered electrolytic ablation (EA) device (Figure 4c. Right) [47]. EA is a non-thermal method in which a localised pH region is created via two electrodes inserted into a tumour and connected to a direct current (DC) source. The EA device consists of an EA microprobe and an ultrasound transmitter, where the EA microprobe has a pair of electrodes and a piezoelectric transducer. During the ablation, an ultrasound transmitter sends high density ultrasound to the EA microprobe, inducing resonance on its piezoelectric transducer, then the piezoelectric transducer will generate DC power to electrodes. An ex-vivo experiment using mice liver was conducted to evaluate the novel device. The experimental results indicated the highest direct voltage and current can be transmitted by piezoelectric transducer was measured to be 5V and 90μA when applying ultrasound with strong ultrasonic intensities (450μW). The wireless power transfer was calculated as 2.7%. The 5V DC power can create an acidic (pH<2) and alkaline (pH>12.9) zone around the catheters. The size of the maximum ablation zone was observed as 0.8cm^3 after an hour at the maximum expansion rate of 0.5mm^3/min. Results from ex-vivo mince experiment

TABLE 2. Variation of impedance parameters in human cancer tissues.

Author	PATHOLOGICAL TISSUE	The frequency range of EIS	Tissue sample size	Referential group 1	Referential group 2
Reihane Mahdavi et al [17]	Ex-vivo Lymph node tissue from breast cancer patients	1kHz	Tumour size: 20 to 50 mm	Z_{1kHz}(Impedance magnitude at 1kHz) **LN involved breast cancer Z_{1kHz}:** Less than 2.3kΩ	**LN not involved breast cancerZ_{1kHz}:**1.8 kΩ to 7.5 kΩ
Ho-Jung Jeong [21]	Ex-vivo Cancerous urothelial cells	10kHz to 1MHz	Cell density of fluid sample $4x10^6$/mL	**Normal urothelial cells** $Re[Z]$: 24.53± 0.75kΩ (10kHz); 3.661 ± 0.8 kΩ (50kHz);1.474 ± 0.26 kΩ(100kHz); 0.362 ± 0.027 kΩ (500kHz); 0.2354 ± 0.053 (1MHz). **Cancerous urothelial cells** $Im[Z]$24.63 ± 0.5 kΩ (10kHz); 3.86 ± 0.2 kΩ(50kHz); 1.57 ± 0.16 kΩ (100kHz);0.374 ± 0.012 kΩ (500kHz); 0.239 ± 0.06 (1MHz)	**Normal urothelial cells** $Re[Z]$: -119.6±0.5 kΩ (10kHz); -31.34±0.35 kΩ (50kHz); -16.8±0.9 kΩ (100kHz); -3.52±0.03 kΩ (500kHz); -1.813±0.003 kΩ(1MHz). **Cancerous urothelial cells** $Im[Z]$: -119.2±0.5 kΩ (10kHz); -31.25±0.15 kΩ(50kHz); 16.52±0.5 -3.53±0.08 kΩ(500kHz) ; -1.808±0.01 kΩ(1MHz)
Sanna Halonen et al. [23]	In-vivo human cancerous liver tissues from 26 patients	1kHz to 100kHz	N/A	**Normal liver (M):** 14kΩ decrease to 2.5kΩ **Normal liver (θ):** -55° increase to -14°	**Liver tumour (M):** 12.5kΩ decrease to 2.4kΩ **Liver tumour (θ):** -60.3° increase to -13°
V. Mishra et al.[20]	Ex-vivo 367 Benign prostate tissue cores (with a mean length of 9.9±6.0 cm); 39 Cancer prostate core. (with a mean length of 3.57±2.95 cm)	1Hz to 100kHz	Mean length of Ex-vivo 367 Benign prostate tissue cores: 9.9±6.0 cm); Mean length of 39 Cancer prostate core: 3.57±2.95 cm.	**ρ_R: Benign (Mean value)** —— 42.8 ± 43.8 Ω-m (100Hz) decrease to 2.4 ± 3.0 Ω -m (1MHz) **ρ_X: Benign (Mean value)** —— 49.7 ± 52.5 Ω-m (100Hz) decrease to -1.1 ± 1.7V Ω-m (1MHz)	**ρ_R: Cancer (Mean value)** ——67.8 ± 48.3 Ω-m (100Hz) decrease to 4.5 ± 24.04 Ω -m(1MHz) **ρ_X: Cancer (Mean value)** —— 92.8 ± 91.2 Ω-m(100Hz) decreased to -4.48 ± 4.96 Ω-m(1MHz)
Giseok Kang et al. [16]	Ex-vivo Human grade I, II, and III cancerous breast tissues	1kHz to 1MHz	Sample size: $27mm^3$	**Passivation type EIS needle:** X_C (Ω): Grade I breast cancer ——7.5 ± 0.3kΩ to 105 ± 5Ω; Grade II breast cancer —— 3.5 ± 0.2kΩ to 50 ± 5 Ω; Grade III breast cancer —— 4k ± 0.2 kΩ to 52 ± 5Ω. X_L (Ω): Grade I breast cancer ——710 ± 10kΩ to 90± 5 kΩ; Grade II breast cancer —— 800 ± 20kΩ to 90 ± 5kΩ; Grade III breast cancer —— 4k ± 0.2 kΩ to 52 ± 5Ω.	**Open-type EIS needle** X_C (Ω): Grade I breast cancer —— 7.8 ± 0.2kΩ to 70 ± 5 Ω; Grade II breast cancer —— 2.8 ± 0.2kΩ to 55 ± 3 Ω; Grade III breast cancer —— 3.3 ± 0.5kΩ to 52 ± 2Ω. X_L (Ω): Grade I breast cancer —— 750 ± 10 kΩ to 85 ± 2kΩ; Grade II breast cancer —— 900 ± 50kΩ to 90 ± 5 kΩ; Grade III breast cancer —— 3.3 ± 0.5kΩ to 52 ± 2Ω.
Joho Yun et al. [14]	Renal cell carcinoma tissues	1kHz to 1MHz	A ex-vivo renal tissue specimen	**M(Ω):** Normal tissue —— 959.05kΩ to 4.08kΩ. **θ:** Normal tissue —— -70° to 67.5°.	**M(Ω):** Cancerous tissue: 1.03MΩ to 4.86MΩ. **θ:** Cancer tissue: -74.69° to -35.58°.
Jinhwan Kim et al. [31]	Ex-vivo cirrhotic liver	1kHz to 1MHz	AN ex-vivo normal liver specimen and a cirrhotic liver specimen	$Re[Z]$: CLP —— 29 ± 2 kΩ to 3.5 ± 5 kΩ; HCC —— 26 ± 2 kΩ to 2.3 ± 2 kΩ; NLP —— 25 ± 2 kΩ to 3.1 ± 0.3kΩ; MTN —— 16 ± 2 kΩ to 1.4 ± 0.3 kΩ.	$Im[Z]$: CLP —— 170 ± 5kΩ to 1.3 ± 0.2 kΩ; HCC —— 175 ± 5kΩ to 1.6 ± 0.2 kΩ; NPL —— 105 ± 2kΩ to 1.6 ± 0.1kΩ; MTN —— 105 ± 2kΩ to 450 ± 10Ω.
Joho Yun et al. [13]	Thyroid cancer tissue	1Hz to 1MHz	Tumour size ≤ 2mm	**PTC** $Re[Z]$ at 251kHz: 1.76kΩ. $Im[Z]$ at 1MHz:357kΩ M at 631kHz: 1.6 kΩ θ at 15.9kHz:44°.	**Normal thyroid tissue** $Re[Z]$ at 251kHz: 1.27 kΩ. $Im[Z]$:220 kΩ M 631kHz: 1.25 kΩ θ at 15.9kHz:50°.

indicated that a single EA microprobe could kill the cancer cells in a maximum number of 1394 spots (± 241 spots).

V. LIMITATION AND FUTURE WORK

A. APPLICATIONS OF CONVENTIONAL SENSING NEEDLES AND BIOIMPEDANCE ANALYSIS METHODS

The EIS data are massive and complicated. It is difficult for doctors or surgeons to understand impedance variation during surgeries or procedures. Therefore, developing an exemplary Graphic User Interface (GUI) and algorithm for sensing needle systems is beneficial for training surgeons, and a good display provides more accurate information for the surgeon to confirm the position of the lesion tissue. Besides, computerised tomography scanning, ultrasound guidance might be used during the insertion of the sensing needle to establish know the position. However, most For the RF ablation needle systems, an exemplary GUI for the RF needles to monitor the temperature and pressure of inner tissue to avoid the ''steam pop'' effect during therapy. Furthermore, 2D-ICE has been validated as a potential method to give clinical staff guidance on the needle position and control the size of the ablated lesion in the patient's body.

B. FABRICATION AND COST

Novel needles comprised of new Au microelectrode were evaluated as having higher sensitivity. However, integrating micro-electrode on the needles require high precision manufacturing by photolithography and a series of complicated processes. Although the reports did not mention the cost of fabricating a needle, complicated fabrication may raise the biopsy needle's price, especially as biopsy needles are often employed as single-use devices. Therefore, finding a simplified and low-cost sensor manufacturing method might make these novel sensing needles more practical. 4-electrode

or multiple microelectrode arrays on the needle should be researched in the future because the 2-electrode needle is easily affected by EP.

C. EIS ANALYSIS FOR TISSUE DISCRIMINATION

The impedance spectrums of different, specifically pathological tissues are different. The impedance spectrums of different, specifically pathological tissues are different. However, most of experimental results in this paper were based on ex-vivo human tissue experiments and obtained by bipolar impedance sensing needle, they might have less referential for practical therapy and measurement error caused by tissue EP. Therefore, current study in this paper is more focused on device fabrication and evaluation, future works should focus on evaluations in practically clinical tests, and the improvement of the measurement accuracy of sensing instruments, respectively.

Training ML models to learn the EIS library and provide accurate diagnosis might be a sensible approach. Conversely, researching and applying more novel sensors on sensing needles to detect pathological tissue pH, glucose concentration, and other ion concentrations has higher potential for clinical diagnosis, especially in cancer biopsy diagnosis.

D. NEEDLE-BASED ABLATION DEVICE

More innovative RFA needles should be researched to predict the occurrence of ''steam pop''. EA provides another option to avoid this. However, a shorter ablation time of the EA ablation system is required. Furthermore, the maximum ablation region needs to be improved in the future. Wireless powering of RF needles provides more convenience for lesion ablation, nevertheless, further improvements of the power transfer efficiency of inductance coils provides higher potential.

VI. CONCLUSION

In this review we have introduced a few tissue discriminations. The majority of studies distinguish pathological tissue by analysing the variations of impedance parameters, including phase angle, real and imaginary part of impedance, versus different frequency ranges. Some reports mentioned that the apparent impedivity can also be used as a classification parameter. Most studies related to clinical trials analysed the electrical properties of bio-tissues below 1MHz. They indicated the optimal frequency for tissue discrimination differs for each impedance parameter. Many cancerous tissue detection methods were developed using EIS data, including ELS, ML, and PCA analysis. They provide good capability and specificity for detecting pathological tissues. Generally, the impedance magnitude of cancerous tissues was recorded to be less than normal tissues, whereas the phase angle of cancer and normal tissue contribute less differences for tissue discrimination. High sweeping frequency range (around 1MHz) presents more impedance differences than that of low sweeping frequency range (under 100kHz). Non-impedance variables such as pH and glucose concentration has also been evaluated for cancer detection. Moreover, impedance sensing needles can replace conventional navigation as a high-accuracy needle guidance in intra-articular space, PIVC, intravenous therapy and eye vessel surgery.

Many commercialized bipolar sensing needles, including IQ-Biopsy, EMG, and BARD biopsy needles, have been shown to perform well in tissue classification. Most novel bipolar sensing needles integrated Au microelectrode have been evaluated to provide higher sensitivity. However, the bipolar electrode has a drawback that it can be affected by EP during impedance sensing. Therefore, 4-electrode sensing needle was evaluated as having capability to decrease the effect from EP during bioimpedance sensing. Novel sensors on the needle such as IrOx-based pH and enzymatic glucose sensors provide more potential in cancer diagnosis. All the novel sensing needle integrated micro-electrode by photolithography, which may increase the cost of their fabrication. Furthermore, most of were not evaluated by clinical experiments. Therefore, novel sensing needles need further research for practical applications.

Electromagnetic induction wirelessly powering RF ablation devices can reduce the risk of wires being damaged or ''shorted'' and provide convenience for clinicians, but their power transmission efficiency need further improvement. Applying sensors on the RF needle and using 2D-ICE can detect ''steam pops'' and monitor the ablation zone, respectively. EA systems provided a non-thermal ablation method, but at present further improvement of its ablation time and zones is required.

DATA AVAILABILITY STATEMENT

The datasets generated and/or analysed during the current study are not publicly available due this is a review paper but are available from the corresponding author on reasonable request.

REFERENCES

[1] B. S. Chhikara and K. Parang, ''Global cancer statistics 2022: The trends projection analysis,'' *Chem. Biol. Lett.*, vol. 10, no. 1, p. 451, 2022.

[2] K. D. Miller, L. Nogueira, T. Devasia, A. B. Mariotto, K. R. Yabroff, A. Jemal, J. Kramer, and R. L. Siegel, ''Cancer treatment and survivorship statistics, 2022,'' *CA, A Cancer J. Clinicians*, vol. 72, no. 5, pp. 409–436, Sep. 2022.

[3] R. Etzioni, N. Urban, S. Ramsey, M. McIntosh, S. Schwartz, B. Reid, J. Radich, G. Anderson, and L. Hartwell, ''The case for early detection,'' *Nature Rev. Cancer*, vol. 3, no. 4, pp. 243–252, 2003.

[4] M. Santarpia, A. Liguori, A. D'Aveni, N. Karachaliou, M. Gonzalez-Cao, M. G. Daffina, C. Lazzari, G. Altavilla, and R. Rosell, ''Liquid biopsy for lung cancer early detection,'' *J. Thoracic Disease*, vol. 10, p. 882, Apr. 2018.

[5] S. F. Shariat and C. G. Roehrborn, ''Using biopsy to detect prostate cancer,'' *Rev. Urol.*, vol. 10, no. 4, p. 262, 2008.

[6] V. Kasivisvanathan, A. S. Rannikko, M. Borghi, V. Panebianco, L. A. Mynderse, M. H. Vaarala, A. Briganti, L. Budäus, G. Hellawell, R. G. Hindley, and M. J. Roobol, ''MRI-targeted or standard biopsy for prostate-cancer diagnosis,'' *New England J. Med.*, vol. 378, no. 19, pp. 1767–1777, 2018.

[7] S. Kimura, T. Morimoto, T. Uyama, Y. Monden, Y. Kinouchi, and T. Iritani, ''Application of electrical impedance analysis for diagnosis of a pulmonary mass,'' *Chest*, vol. 105, no. 6, pp. 1679–1682, Jun. 1994.

[8] S. Khalil, M. Mohktar, and F. Ibrahim, "The theory and fundamentals of bioimpedance analysis in clinical status monitoring and diagnosis of diseases," *Sensors*, vol. 14, no. 6, pp. 10895–10928, Jun. 2014.

[9] S. B. Rutkove, R. Aaron, and C. A. Shiffman, "Localized bioimpedance analysis in the evaluation of neuromuscular disease," *Muscle Nerve*, vol. 25, no. 3, pp. 390–397, Mar. 2002.

[10] Y. H. Shash, M. A. A. Eldosoky, and M. T. Elwakad, "The effect of vascular diseases on bioimpedance measurements: Mathematical modeling," *Biomed. Res. Therapy*, vol. 5, no. 6, pp. 2414–2431, Jun. 2018.

[11] R. Crescenzi, P. M. C. Donahue, S. Weakley, M. Garza, M. J. Donahue, and K. L. Herbst, "Lipedema and Dercum's disease: A new application of bioimpedance," *Lymphatic Res. Biol.*, vol. 17, no. 6, pp. 671–679, Dec. 2019.

[12] C. Carpano Maglioli, D. G. Caldwell, and L. S. Mattos, "A bioimpedance sensing system for in-vivo cancer tissue identification: Design and preliminary evaluation," in *Proc. 39th Annu. Int. Conf. IEEE Eng. Med. Biol. Soc. (EMBC)*, Jul. 2017, pp. 4235–4238.

[13] J. Yun, Y.-T. Hong, K.-H. Hong, and J.-H. Lee, "Ex vivo identification of thyroid cancer tissue using electrical impedance spectroscopy on a needle," *Sens. Actuators B, Chem.*, vol. 261, pp. 537–544, May 2018.

[14] J. Yun, H. W. Kim, Y. Park, J.-J. Cha, J. Z. Lee, D. G. Shin, and J.-H. Lee, "Micro electrical impedance spectroscopy on a needle for ex vivo discrimination between human normal and cancer renal tissues," *Biomicrofluidics*, vol. 10, no. 3, May 2016, Art. no. 034109.

[15] V. Mishra, A. Schned, A. Hartov, J. Heaney, J. Seigne, and R. Halter, "Electrical property sensing biopsy needle for prostate cancer detection," *Prostate*, vol. 73, no. 15, pp. 1603–1613, 2013.

[16] G. Kang, J. Yun, J. Cho, J. Yoon, and J. Lee, "Micro electrical impedance spectroscopy (μEIS) fabricated on the curved surface of a fine needle for biotissue discrimination," *Electroanalysis*, vol. 28, no. 4, pp. 733–741, Apr. 2016.

[17] R. Mahdavi, N. Yousefpour, F. Abbasvandi, H. Ataee, P. Hoseinpour, M. E. Akbari, M. Parniani, B. Delshad, M. Avatefi, Z. Nourinejad, S. Abdolhosseini, S. Mehrvarz, F. Hajighasemi, and M. Abdolahad, "Intra-operative pathologically-calibrated diagnosis of lymph nodes involved by breast cancer cells based on electrical impedance spectroscopy; A prospective diagnostic human model study," *Int. J. Surg.*, vol. 96, Dec. 2021, Art. no. 106166.

[18] V. S. Teixeira, W. Krautschneider, and J. J. Montero-Rodriguez, "Bioimpedance spectroscopy for characterization of healthy and cancerous tissues," in *Proc. IEEE Int. Conf. Electr. Eng. Photon.*, Oct. 2018, pp. 147–151.

[19] R. Baghbani, M. B. Shadmehr, M. Ashoorirad, S. F. Molaeezadeh, and M. H. Moradi, "Bioimpedance spectroscopy measurement and classification of lung tissue to identify pulmonary nodules," *IEEE Trans. Instrum. Meas.*, vol. 70, pp. 1–7, 2021.

[20] V. Mishra, H. Bouayad, A. Schned, A. Hartov, J. Heaney, and R. J. Halter, "A real-time electrical impedance sensing biopsy needle," *IEEE Trans. Biomed. Eng.*, vol. 59, no. 12, pp. 3327–3336, Dec. 2012.

[21] H.-J. Jeong, K. Kim, H. W. Kim, and Y. Park, "Classification between normal and cancerous human urothelial cells by using micro-dimensional electrochemical impedance spectroscopy combined with machine learning," *Sensors*, vol. 22, no. 20, p. 7969, Oct. 2022.

[22] A. Gaur, J. Sharp, K. Bouazza-Marouf, and D. Noronha, "Tissue type determination by impedance measurement: A bipolar and monopolar comparison," *Saudi J. Anaesthesia*, vol. 11, no. 1, p. 15, 2017.

[23] S. Halonen, A. Ovissi, S. Boyd, J. Kari, K. Kronström, J. Kosunen, H. Laurén, K. Numminen, H. Sievänen, and J. Hyttinen, "Human in vivo liver and tumor bioimpedance measured with biopsy needle," *Physiological Meas.*, vol. 43, no. 1, Jan. 2022, Art. no. 015006.

[24] Z. Cheng, A. L. C. Carobbio, L. Soggiu, M. Migliorini, L. Guastini, F. Mora, M. Fragale, A. Ascoli, S. Africano, D. G. Caldwell, F. R. M. Canevari, G. Parrinello, G. Peretti, and L. S. Mattos, "Smart-Probe: A bioimpedance sensing system for head and neck cancer tissue detection," *Physiological Meas.*, vol. 41, no. 5, Jun. 2020, Art. no. 054003.

[25] J. Park, W.-M. Choi, K. Kim, W.-I. Jeong, J.-B. Seo, and I. Park, "Biopsy needle integrated with electrical impedance sensing microelectrode array towards real-time needle guidance and tissue discrimination," *Sci. Rep.*, vol. 8, no. 1, pp. 1–12, Jan. 2018.

[26] J. Park, Y. Jeong, J. Kim, J. Gu, J. Wang, and I. Park, "Biopsy needle integrated with multi-modal physical/chemical sensor array," *Biosensors Bioelectron.*, vol. 148, Jan. 2020, Art. no. 111822.

[27] H. Kwon, J. F. Di Cristina, S. B. Rutkove, and B. Sanchez, "Recording characteristics of electrical impedance-electromyography needle electrodes," *Physiological Meas.*, vol. 39, no. 5, May 2018, Art. no. 055005.

[28] H. Kalvøy and A. R. Sauter, "Detection of intraneural needle-placement with multiple frequency bioimpedance monitoring: A novel method," *J. Clin. Monitor. Comput.*, vol. 30, no. 2, pp. 185–192, Apr. 2016.

[29] M. A. Abbasi, H. Kim, S. R. Chinnadayyala, K. D. Park, and S. Cho, "Real-time impedance detection of intra-articular space in a porcine model using a monopolar injection needle," *Sensors*, vol. 20, no. 16, p. 4625, Aug. 2020.

[30] J. Yun, G. Kang, Y. Park, H. W. Kim, J.-J. Cha, and J.-H. Lee, "Electrochemical impedance spectroscopy with interdigitated electrodes at the end of hypodermic needle for depth profiling of biotissues," *Sens. Actuators B, Chem.*, vol. 237, pp. 984–991, Dec. 2016.

[31] J. Kim, J. Yun, K. Kim, N. I. Kim, H. J. Kim, and J.-H. Lee, "Ex-vivo identification of tumor from parenchyma in human liver using electrochemical impedance spectroscopy on a needle," *IEEE Sensors J.*, vol. 20, no. 23, pp. 14042–14049, Dec. 2020.

[32] W. H. Koppenol and P. L. Bounds, "The Warburg effect and metabolic efficiency: Re-crunching the numbers," *Science*, vol. 324, no. 5930, pp. 1029–1033, 2009.

[33] R. K. Jain, "Delivery of molecular medicine to solid tumors: Lessons from in vivo imaging of gene expression and function," *J. Controlled Release*, vol. 74, nos. 1–3, pp. 7–25, Jul. 2001.

[34] G. Yuge, W. Hanbin, Z. Yan, and L. Li, "Research progress on the mechanisms of chemotherapy resistance to glioblastoma in-duced by hypoxia microenvironment," *Chin. J. Clin. Oncol.*, vol. 44, no. 21, pp. 1100–1103, 2017.

[35] E. L. Pearce, M. C. Poffenberger, C.-H. Chang, and R. G. Jones, "Fueling immunity: Insights into metabolism and lymphocyte function," *Science*, vol. 342, no. 6155, Oct. 2013, Art. no. 1242454.

[36] R. Lin, Y. Jin, R. R. Li, C. Jiang, J. Ping, C. J. Charles, Y. L. Kong, and J. S. Ho, "Needle-integrated ultrathin bioimpedance microsensor array for early detection of extravasation," *Biosensors Bioelectron.*, vol. 216, Nov. 2022, Art. no. 114651.

[37] Z. Cheng, B. L. Davies, D. G. Caldwell, and L. S. Mattos, "A new venous entry detection method based on electrical bio-impedance sensing," *Ann. Biomed. Eng.*, vol. 46, no. 10, pp. 1558–1567, Oct. 2018.

[38] L. Schoevaerdts, L. Esteveny, A. Gijbels, J. Smits, D. Reynaerts, and E. V. Poorten, "Design and evaluation of a new bioelectrical impedance sensor for micro-surgery: Application to retinal vein cannulation," *Int. J. Comput. Assist. Radiol. Surg.*, vol. 14, no. 2, pp. 311–320, Feb. 2019.

[39] J. Moore, K. Nilsson, B. Wood, S. Xu, and Z. T. Ho Tse, "Liver radiofrequency ablation using wirelessly powered catheter and generator," in *Proc. IEEE PELS Workshop Emerg. Technol., Wireless Power Transf. (Wow)*, Jun. 2018, pp. 1–5.

[40] J. Moore, S. Xu, B. J. Wood, H. Ren, and Z. T. H. Tse, "Radiofrequency tumor ablation system with a wireless or implantable probe," *Wireless Power Transf.*, vol. 7, no. 2, pp. 95–105, Sep. 2020.

[41] M. Wallace, M. Moris, M. Atar, A. Kadayifci, M. Krishna, A. Librero, E. Richie, and W. Brugge, "Thermal ablation of pancreatic cyst with a prototype endoscopic ultrasound capable radiofrequency needle device: A pilot feasibility study," *Endoscopic Ultrasound*, vol. 6, no. 2, p. 123, 2017.

[42] J. Dickow, S. Wang, A. Suzuki, K. Imamura, H. I. Lehmann, K. D. Parker, L. K. Newman, K. H. Monahan, M. E. Rettmann, M. G. Curley, and D. L. Packer, "Real-time intracardiac echocardiography validation of saline-enhanced radiofrequency needle-tip ablation: Lesion characteristics and gross pathology correlation," *EP Europace*, vol. 23, no. 11, pp. 1826–1836, Nov. 2021.

[43] J. Park, D. I. Cha, Y. Jeong, H. Park, J. Lee, T. W. Kang, H. K. Lim, and I. Park, "Real-time internal steam pop detection during radiofrequency ablation with a radiofrequency ablation needle integrated with a temperature and pressure sensor: Preclinical and clinical pilot tests," *Adv. Sci.*, vol. 8, no. 19, Oct. 2021, Art. no. 2100725.

[44] T. Livraghi, S. N. Goldberg, S. Lazzaroni, F. Meloni, L. Solbiati, and G. S. Gazelle, "Small hepatocellular carcinoma: Treatment with radio-frequency ablation versus ethanol injection," *Radiology*, vol. 210, no. 3, pp. 655–661, Mar. 1999.

[45] K. Kotoh, "Scattered and rapid intrahepatic recurrences after radio frequency ablation for hepatocellular carcinoma," *World J. Gastroenterol.*, vol. 11, no. 43, p. 6828, 2005.

[46] K. Kotoh, M. Nakamuta, S. Morizono, M. Kohjima, E. Arimura, M. Fukushima, M. Enjoji, H. Sakai, and H. Nawata, "A multi-step, incremental expansion method for radio frequency ablation: Optimization of the procedure to prevent increases in intra-tumor pressure and to reduce the ablation time," *Liver Int.*, vol. 25, no. 3, pp. 542–547, Jun. 2005.
[47] A. Kim, S. K. Lee, T. Parupudi, R. Rahimi, S. H. Song, M. C. Park, S. Islam, J. Zhou, A. K. Majumdar, J. S. Park, J. M. Yoo, and B. Ziaie, "An ultrasonically powered implantable microprobe for electrolytic ablation," *Sci. Rep.*, vol. 10, no. 1, pp. 1–9, Jan. 2020.

YIJIANG HU received the Bachelor of Engineering degree in electronic and communication engineering from the University of York. He is currently pursuing the Ph.D. degree in medical engineering with the Digital Health and Robotics Laboratory, Queen Mary University of London, with a focus on needle-based diagnostic and therapeutic technologies for oncological applications.

CHAYABHAN LIMPABANDHU received the Bachelor of Engineering degree in electronics and communication engineering from the Sirindhorn International Institute of Technology, Thammasat University, and the Master of Science degree in intelligence systems and robotics from the University of Essex. She is currently pursuing the Ph.D. degree in medical engineering with the Digital Health and Robotics Laboratory, Queen Mary University of London, with a focus on magnetically actuated devices for medical interventions. Her academic journey and professional experiences are deeply rooted in the advancement of medical device technology, particularly in the integration of robotics and magnetic actuation in healthcare applications. Her contributions to interdisciplinary projects and academic competitions highlight her dedication to innovation in the fields of digital health and medical engineering.

TRISTAN BARRETT is currently an Associate Professor with the Department of Radiology, University of Cambridge, and an Honorary NHS Consultant Radiologist. His main research interest includes prostate cancer, with a particular interest in multi-parametric MRI techniques for identifying and characterizing prostate tumors.

ZION TSZ HO TSE received the Ph.D. degree in mechatronics in medicine from Imperial College London, U.K. He is currently an Academy of Medical Sciences Professor of digital health and robotics and the Director of the Centre for Bioengineering, Queen Mary University of London. Before that, he was a Chair Professor with the University of York and an Associate Professor with the University of Georgia. Before that, he was a Research Fellow with Harvard University, Boston, MA, USA. Most of his academic and professional experience has been in AI, digital health, medical robotics, and imaging. He has been developing and testing a broad range of medical technologies in his career, most of which have been applied in clinical patient trials. His research bridges engineering and medicine, connecting multidisciplinary teams of medical doctors, researchers, and engineers.